Thesis for the Degree of Licentiate of Engineering

Factorized Geometrical Autofocus for Synthetic Aperture Radar Processing

Jan Torgrimsson

CHALMERS

Department of Earth and Space Sciences
Chalmers University of Technology
Gothenburg, Sweden 2013

Factorized Geometrical Autofocus for Synthetic Aperture Radar Processing

Jan Torgrimsson

Technical Report 55L,
Radar Remote Sensing Group
Department of Earth and Space Sciences
Chalmers University of Technology
SE–412 96 Gothenburg, Sweden
Phone: +46 (0)31 772 1000
E-mail: tojan@chalmers.se

Printed by Chalmers Reproservice
Chalmers University of Technology
Gothenburg, Sweden 2013

Factorized Geometrical Autofocus for Synthetic Aperture Radar Processing

Jan Torgrimsson
Department of Earth and Space Sciences
Chalmers University of Technology

Abstract

Synthetic Aperture Radar (SAR) imagery is a very useful resource for the civilian remote sensing community and for the military. This however presumes that images are focused. There are several possible sources for defocusing effects. For airborne SAR, motion measurement errors is the main cause. A defocused image may be compensated by way of autofocus, estimating and correcting erroneous phase components.

Standard autofocus strategies are implemented as a separate stage after the image formation (stand-alone autofocus), neglecting the geometrical aspect. In addition, phase errors are usually assumed to be space invariant and confined to one dimension. The call for relaxed requirements on inertial measurement systems contradicts these criteria, as it may introduce space variant phase errors in two dimensions, i.e. residual space variant Range Cell Migration (RCM).

This has motivated the development of a new autofocus approach. The technique, termed the Factorized Geometrical Autofocus (FGA) algorithm, is in principle a Fast Factorized Back-Projection (FFBP) realization with a number of adjustable (geometry) parameters for each factorization step. By altering the aperture in the time domain, it is possible to correct an arbitrary, inaccurate geometry. This in turn indicates that the FGA algorithm has the capacity to compensate for residual space variant RCM.

In appended papers the performance of the algorithm is demonstrated for geometrically constrained autofocus problems. Results for simulated and real (Coherent All RAdio BAnd System II (CARABAS II)) Ultra WideBand (UWB) data sets are presented. Resolution and Peak to SideLobe Ratio (PSLR) values for (point/point-like) targets in FGA and reference images are similar within a few percents and tenths of a dB.

As an example: the resolution of a trihedral reflector in a reference image and in an FGA image respectively, was measured to approximately 3.36 m/3.44 m in azimuth, and to 2.38 m/2.40 m in slant range; the PSLR was in addition measured to about 6.8 dB/6.6 dB.

The advantage of a geometrical autofocus approach is clarified further by comparing the FGA algorithm to a standard strategy, in this case the Phase Gradient Algorithm (PGA).

Keywords: Autofocus, Back-Projection, FGA, PGA, SAR, UWB

Appended papers

This thesis is based on the papers below:

Paper A: H. Hellsten, **J. Torgrimsson**, P. Dammert, L. M. H. Ulander and A. Åhlander. Evaluation of a geometrical autofocus algorithm within the framework of Fast Factorized Back-Projection. *Proceedings of IET Radar 2012*, Glasgow, Scotland, 22–25 October 2012

Paper B: **J. Torgrimsson**, P. Dammert, H. Hellsten and L. M. H. Ulander. Factorized Geometrical Autofocus for Synthetic Aperture Radar Processing. Submitted to *IEEE Transactions on Geoscience and Remote Sensing*, February 2013.

Related papers

The paper below is a feasibility study, not appended in this thesis:

Paper I: **J. Torgrimsson**. Evaluation of a new autofocus algorithm within the framework of Fast Factorized Back-Projection. Technical report No. 8, 70 pages, Department of Earth and Space Sciences, Chalmers University of Technology, November, 2011.

Acknowledgement

- I would like to thank my supervisor: Lars Ulander, my assistant supervisor: Leif Eriksson, and of course my colleagues and former colleague in the Radar Remote Sensing Group: Maciej, Anders, Gustaf, Gisela and Annelie, for all their help and support.
- A special thanks to my assistant supervisor at SAAB Electronic Defence Systems (EDS): Patrik Dammert, for great guidance and very interesting weekly discussions.
- Also, many thanks to: Hans Hellsten, Anders Åhlander and Jonas Lindgren at SAAB EDS.

Index

Chapter 1

Introduction

1.1 Synthetic Aperture Radar (SAR)

Synthetic Aperture Radar (SAR) is a technology used to form high-resolution imagery [3, 5, 27]. The fundamental idea, originating from the early 50's, is to simulate a very large antenna, put into practice by recording radar echoes at multiple positions along a track and combining these coherently.

After processing raw data, an image with pixels in range and cross-range (or azimuth/along-track)[1] is obtained, in principle reproducing the reflectivity of the scene.

SAR imaging has many advantages, day/night capability is one, as radar supplies its own illumination. All-weather capability is another, as ElectroMagnetic (EM) waves at radar frequencies (see table 1.1) generally penetrate through clouds and precipitation. Additionally, a SAR image often provides a different view of a given target compared to an optical representation, i.e. due to disparate scattering mechanisms.

Air- and spaceborne SAR systems are widely applied by the remote sensing community, for mapping, land-use surveying, planetary investigation, etc., and by the military, for reconnaissance, surveillance, etc.

The coming discussion will deal with the resolution concept. A typical SAR geometry (stripmap mode) is shown in figure 1.1 to support the review. It is assumed that an airborne platform travels along a linear track at constant altitude, above a horizontal ground plane. Echoes are recorded at equidistant positions, during pulse transmission/reception the platform is presumed to be stationary, i.e. the start-stop approximation [36] is adopted. A constant wave velocity and a valid Born approximation are additional premises [36].

Band	Frequency (GHz)
HF	0.003-0.03
VHF	0.03-0.3
UHF (P)	0.3-1
L	1-2
S	2-4
C	4-8
X	8-12
Ku	12-18
K	18-27
Ka	27-40
V	40-75
W	75-110

Table 1.1: resumes different radar bands [33]. In this thesis the VHF band (and the high HF band) is of primary interest. Namely because the second Swedish Coherent All RAdio BAnd System (CARABAS II) [19] operates in this band (to be more exact between 20-90 MHz, i.e. a 70 MHz bandwidth and a centre frequency at 55 MHz). Data sets acquired by this system have been processed into images, results are presented in paper B.

[1] Cross-range is a direction orthogonal to the (nominal) pointing direction of the (physical) antenna. For a squint angle equal to zero (nominally), cross-range and azimuth/along-track share a common axis, this is assumed from now on.

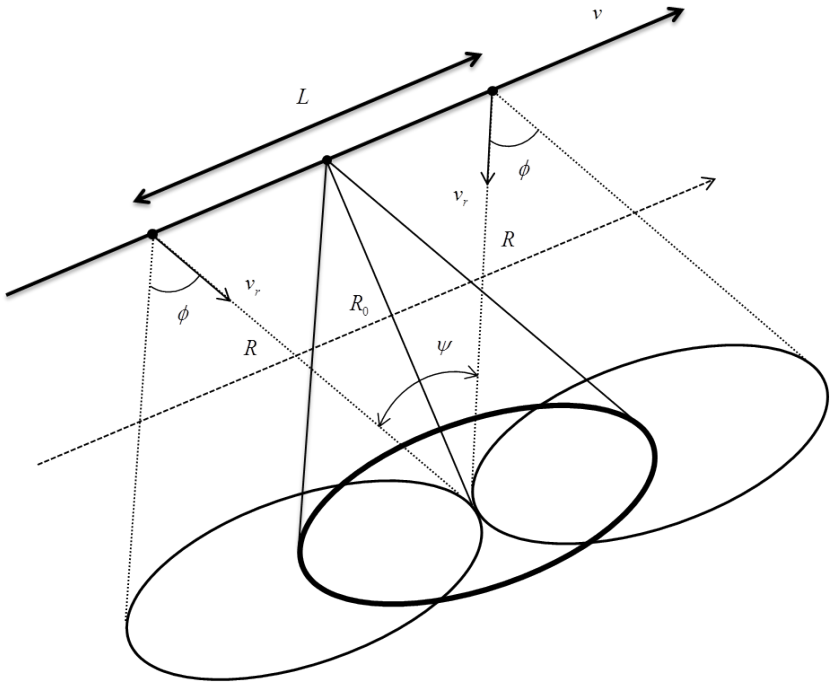

Figure 1.1: shows a SAR geometry where an airborne platform travels at a velocity v along a linear track at constant altitude; the ground is a horizontal Focus Target Plane (FTP). A broadside-looking antenna with beamwidth ϕ illuminates the scene, footprints for three sample positions are illustrated. R_0 represents the slant range of closest approach (broadside at the centre of the synthetic aperture) to a point target. R represents the slant range to the scatterer at the beginning/end of the synthetic aperture. L at last denotes the synthetic aperture length (note also that the target reflects over an integration angle $\psi = \phi$, that v_r equals radial velocity and that range (to the target) follows a hyperbolic function along the track).

Beginning with the basics; a Real Aperture Radar (RAR) has a cross-range resolution of:

$$\Delta_{cr} = \alpha \cdot R_0 \cdot \phi = \alpha \cdot \frac{R_0 \lambda_c}{d} \tag{1.1}$$

In (1.1) λ_c is the centre wavelength of the transmitted signal (EM waves). d denotes the size of the antenna in azimuth, note that the beamwidth (ϕ) is expressed as λ_c/d. α is in turn a factor to account for tapering and different definitions regarding resolution (3-dB, Peak-to-Null, etc.).

It is evident that Δ_{cr} can be enhanced by increasing the EM wave frequency (the centre frequency (f_c) of the transmitted signal) and/or the antenna size (d). However, attenuation restricts the first alternative and the second alternative is constrained physically.

A SAR on the contrary, essentially operates as an array antenna to attain a cross-range resolution of:

$$\Delta_{cr} = \alpha \cdot \frac{R_0 \lambda_c}{2L} \tag{1.2}$$

Assuming that λ_c is fixed, the synthetic aperture length (L) now determines Δ_{cr}.

A Uniform Linear Array (ULA) model[2] may be employed to derive (1.2). The calculation may also be performed from a pulse compression perspective. In this thesis the latter strategy is prefered, as it fits the processing framework later on.

[2] A number of antenna elements, transmitting EM waves simultaneously from equidistant positions (along a line).

It is well-known that a signal with bandwidth B can be compressed to a duration proportional to $1/B$. The bandwidth may be produced by chirping a pulse, the compression is then carried out by convolving the signal with its replica (a time-reversed, complex conjugated signal copy).

In radar, echoes are filtered to reach a range resolution of:

$$\Delta_r = \beta \cdot \frac{c}{2B} \tag{1.3}$$

In (1.3) c signifies the speed of light (the presumed wave propagation velocity), in addition, a factor two in the denominator reflects the two-way propagation path. β is in turn a correspondence to α.

Equation (1.3) reveals the resolvability in slant range for an arbitrary radar system (i.e. RAR as well as SAR), transmitting a signal with bandwidth B. For SAR, a Doppler bandwidth (B_d) is produced as well, due to relative motion between the moving platform (traveling at a velocity v) and stationary targets[3]. Thus, the azimuth resolution may also be expressed as:

$$\Delta_{cr} = \alpha \cdot \frac{v}{B_d} \tag{1.4}$$

For a given target; B_d is the difference in Doppler frequency between the beginning of the synthetic aperture and the end. The Doppler frequency is computed as:

$$f_d = \frac{-2v_r}{\lambda_c} \tag{1.5}$$

By means of (1.5) the Doppler bandwidth for the scatterer in figure 1.1 is deduced:

$$B_d = \frac{4v}{\lambda_c} \cdot \sin(\psi/2) \tag{1.6}$$

In (1.6) ψ is the integration angle. For a SAR system in stripmap mode [5] (see figure 1.1) $\psi = \phi$.
In spotlight mode [3]; the antenna is steered to cover a confined area (not a continuous strip, but a spot or spots) with a wider integration angle, implying finer cross-range resolution[4].

Equation (1.6) is inserted into (1.4), after a small angle approximation:

$$\Delta_{cr} = \alpha \cdot \frac{\lambda_c}{2\psi} \tag{1.7}$$

By means of figure 1.1 the formula below is found:

$$2 \cdot \tan(\psi/2) = \frac{L}{R_0} \tag{1.8}$$

After another small angle approximation, (1.8) is inserted into (1.7), at last rendering (1.2). Finally it should also be stressed, that in stripmap mode; the azimuth resolution may be expressed as:

$$\Delta_{cr} = \alpha \cdot \frac{d}{2} \tag{1.9}$$

[3]The Doppler bandwidth is produced through a phase change (in the received signal) from position to position along the track. Due to the start-stop approximation, platform motion is really an indirect reason for B_d.

[4]In Scan mode [5] an extended swath is illuminated (by scanning the antenna in range),
in consequence degrading the along-track resolution.

Equation (1.9) indicates a range independent Δ_{cr} in stripmap mode, or a range dependent synthetic aperture length. Additionally, (1.9) (as opposed to (1.1)) declares that a finer cross-range resolution can be attained by decreasing the antenna size (d) (i.e. due to a wider beam- and (Doppler) bandwidth). There is however a limit, established by Signal to Noise Ratio (SNR) requirements and range ambiguities.

The presented (SAR) theory ((1.2) to (1.9)) is valid for NarrowBand (NB) systems (narrow integration angle, low relative bandwidth (B/f_c)). For Ultra WideBand (UWB) systems (wide integration angle, high relative bandwidth), e.g. CARABAS II [19], the achievable cross-range resolution is actually a bit finer, the range resolution is in turn coarser[5]. More information is found in [34, 38, 39].

The first section of this thesis has come to an end, paving the way for a processing-oriented discussion, addressing the image formation and different algorithms.

1.2 Image Formation

The purpose of SAR processing is to resolve the scene reflectivity by focusing raw data (see figure 1.2-1.4). This is an inverse problem involving a varying 2-dimensional impulse response [5, 27, 32].

Assume a SAR geometry where an airborne platform travels along an arbitrary (linear or nonlinear) track; a Digital Elevation Map (DEM) gives information regarding ground topography. Note also that general premises still are adopted (i.e. the start-stop and the Born approximation, as well as a constant wave velocity [36]). Additionally, the transmitted signal is presumed to be a chirped pulse, i.e. a time-limited signal with a Linear Frequency Modulation (LFM) or a quadratic phase [5]:

$$s_t(\tau) = w_r(\tau) \cdot \cos(2\pi f_c \tau + \pi k \tau^2) \tag{1.10}$$

In (1.10) τ is the fast-time variable (the time between transmission (start) and reception (stop) at a fixed position along the track), k represents the chirp rate and w_r is the envelope.

The pulse is transmitted at multiple positions (not necessarily equidistant), the slow-time variable η denotes time instants for transmission and reception (fixed platform positions, see start-stop approximation). A point target on the ground reflects the pulse and echoes are recorded, yielding a 2-dimensional impulse response [5]:

$$h_r(\tau, \eta) = w_a(\eta) \cdot w_r(\tau - 2R(\eta)/c) \cdot \cos(2\pi f_c(\tau - 2R(\eta)/c) + \pi k(\tau - 2R(\eta)/c)^2) \tag{1.11}$$

In (1.11) $R(\eta)$ represents the slant range between the platform and the target at different positions (x_η, y_η, z_η) along the track. w_a accounts for the antenna diagram. Note also that (1.11) omits attenuation, range spreading loss, system noise, and possibly, a constant phase change. h_r can be converted to a complex baseband response (h_{bb}) by way of a quadrature demodulation procedure [5]:

$$h_{bb}(\tau, \eta) = w_a(\eta) \cdot w_r(\tau - 2R(\eta)/c) \cdot \exp(-j4\pi f_c R(\eta)/c) \cdot \exp(j\pi k(\tau - 2R(\eta)/c)^2) \tag{1.12}$$

An image ($I(x, y)$) is then specified, presume that pixels constitute ground coordinates. The scene is modeled as a composition of single-scattering objects (i.e. the superposition principle is valid, see Born approximation), for simplicity assume point targets. A matched filter (h_n) may be computed as a time-reversed, conjugated copy of h_{bb}. By filtering baseband data (s_{bb}) with h_n (calculated by means of platform and pixel positions[6]), the image, or equivalent an estimate of the reflectivity, is obtained [27]:

$$I(x, y) = \int_{-\infty}^{\infty} \int_{-\infty}^{\infty} s_{bb}(\tau, \eta)\, h_n(\tau, \eta; x, y)\, d\tau d\eta \tag{1.13}$$

[5] Δ_{cr} and Δ_r differ as the spectral support of the image now must be described by a sector of a circular annulus, contrary to a rectangle or a square. Another way of viewing it, is to regard that the use of λ_c is a rough approximation for wideband signals (large λ span).

[6] Note that a z coordinate can be included in this computation.

Applying a 2-dimensional matched filter (a discrete realization of h_n) [5, 27, 32] on raw data is an accurate and direct processing approach. The strategy can however not benefit from fast convolution, as each pixel defines a different kernel, i.e. the impulse response is space variant. This makes the method too slow to be of practical use.

Fortunately; the inverse problem above has numerous alternative solutions (most of these are however approximate), both time and frequency domain algorithms are available for image formation (see chapter 2). Traditionally though, the frequency domain has been favoured for faster run time.

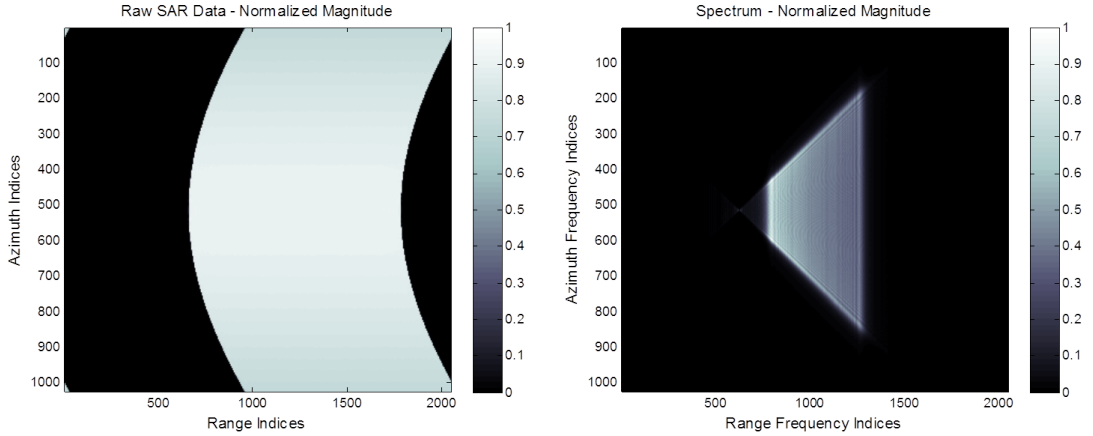

Figure 1.2: shows raw data for a point target (left), the set-up is summarized in figure 1.1. A CARABAS II like system, transmitting a frequency swept (a linear chirp) rectangular pulse, is assumed. Note that range and azimuth indices may be replaced by τ and η. On the right side the spectrum is seen. It is obvious that the Doppler bandwidth (B_d) depends on the transmitted signal (i.e. on the instantaneous frequency).

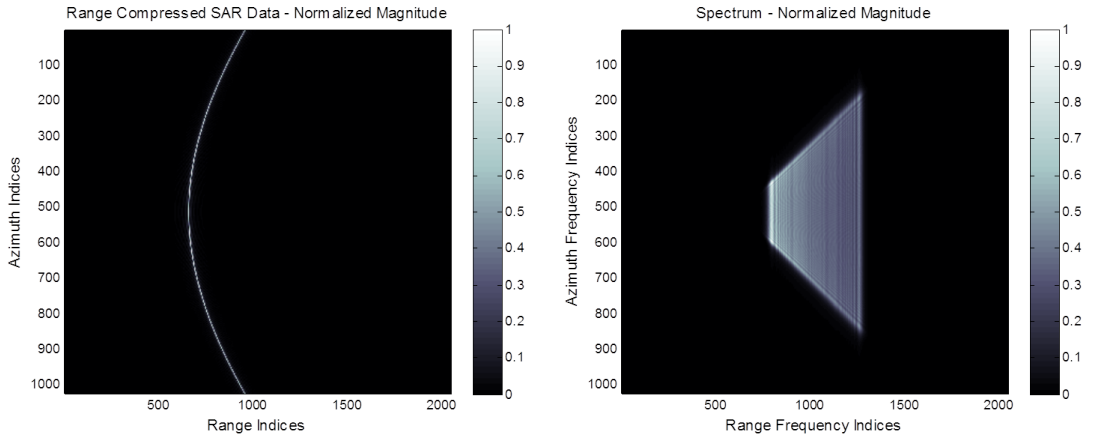

Figure 1.3: shows range compressed data (left), appearing as a thin hyperbolic curve (duration proportional to $1/B$), representing the range to a presumed platform (along the track). In this case the range change across the aperture constitutes several resolution cells. Range Cell Migration (RCM) complicates the processing. The spectrum on the right side looks like the spectrum for raw data, as the compression only alters phase properties. Fundamentally, the transmitted/received signal has a quadratic phase in fast-time and in the frequency domain, canceling this component yields a sinc response.

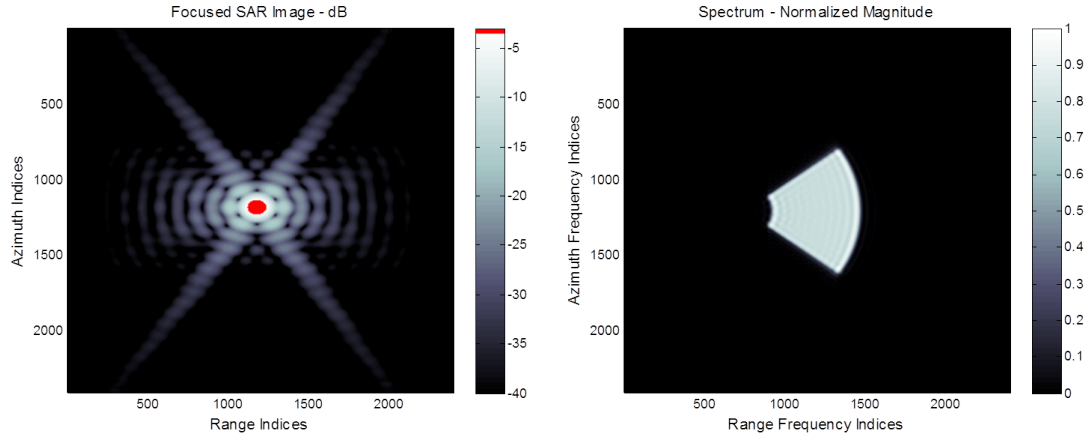

Figure 1.4: shows the final image (left), a close-up of the target, focused (completely compressed) in the time domain through Global Back-Projection (GBP) [1, 8, 12, 27, 32, 36], see chapter 2. Note that the plot has been interpolated 25 times and that the 3-dB area is marked red. Compared to figure 1.2-1.3 (left) the extent is about 100 × 100 pixels. The spectrum (right) is shaped as a (uniform magnitude) sector of a circular annulus, explaining crossed sidelobes (left), a typical UWB attribute.

Processing approximations, motion measurement errors[7], dispersion effects (relevant for spaceborne SAR systems) and erroneous transmitter/receiver quantities (time and phase instabilities), induce faulty phase components, degrading the final image (note though that in the appended papers, an inaccurate geometry is assumed to generate all phase errors).

Different classes (polynomial, sinusoidal and wideband) are usually adopted to describe defocusing phase errors and their impact [3]. A few 1-dimensional examples are provided in the paragraph below.

Quadratic components basically broaden the mainlobe of an impulse (point target) response, leading to a loss of resolution. Cubic components give rise to assymetrical sidelobes, leading to a poor Peak to SideLobe Ratio (PSLR). Single frequency sinusoidal errors, raise sidelobes in pairs (paired echoes), see cubic consequence. Wideband errors ultimately increase the Integrated SideLobe Ratio (ISLR). In all cases, an SNR decrease and a contrast deterioration also follow.

If an inferior image is obtained due to reasons recapped above it must be compensated to be of any use. This is where autofocus normally enters the picture.

In the context of SAR processing, autofocus is the utilization of information in a defocused image to estimate and correct phase errors [3]. Standard algorithms are implemented separately (i.e. stand-alone autofocus) as a 1-dimensional (azimuth) compensation stage. This is often an adequate (not necessarily) and fast approach.

1.3 Thesis Objectives

The first objective (chapter 2) of this thesis is to motivate the advantages of time domain SAR processing, before doing that, frequency domain algorithms are summarized briefly. Two relevant time domain techniques are also resumed, to establish a foundation for the third chapter.

The second and principal objective (chapter 3) is to promote a fully integrated autofocus algorithm[8], realized in the time domain. An overview of the work done in the field so far sets the tone for this task.

Appended papers reveal further details regarding the new autofocus approach, results for simulated and real (CARABAS II) UWB data sets are also presented.

[7] See Global Positioning Systems (GPS), Inertial Navigation Systems (INS) and Inertial Measurement Units (IMU).
[8] Incorporated in a conventional processing chain, contrary to stand-alone autofocus.

Chapter 2

SAR Processing

2.1 Frequency Domain vs. Time Domain

SAR processing techniques can be categorized after domain (stressing where primary processing steps are executed), i.e. as frequency or time domain algorithms. The former category is summarized below, for more information, corresponding references are recommended.

Fundamental frequency domain techniques such as Doppler Beam Sharpening (DBS) [27] and the rectangular algorithm [5] presume that the maximum range change across the aperture never exceeds half the width of a resolution cell (Δ_r). Concisely, RCM is not mitigated. If the condition is satisfied, the processing can be divided into two 1-dimensional (fast convolution) routines[1], i.e. separate range and azimuth compression, saving time.

The next sophistication level adds (approximate) RCM Correction (RCMC) and (often) compensation for cross coupling effects[2]. Examples of techniques are: the Polar Format Algorithm[3] (PFA) [3, 21, 32, 41], the Range Doppler Algorithm (RDA) [5], the Chirp Scaling Algorithm (CSA) [3,5,6,26,29] and various extended CSA variants [7, 24, 25, 37]. Listed techniques trade speed for accuracy. The RDA for instance, employs an interpolation scheme as an intermediate stage between range and azimuth compression (in the range time and azimuth frequency or Range Doppler (RD) domain[4]) to correct RCM. The CSA is in turn a comparable or better alternative to elaborate RDA versions (regarding performance). The advantage of this algorithm is that it only requires phase multiplications (in the RD domain and in the 2-dimensional frequency domain), implying implementation efficiency.

Ultimately, Fourier Hankel inversion [1, 12, 17] is the most exact (frequency domain) method. In practice though, a capable approximation denominated as the Range Migration Algorithm (RMA) (or the ΩK Algorithm (ΩKA)) [2, 3, 5, 28, 32] is used, compressing targets (in the 2-dimensional frequency domain) by way of a reference multiplication and a range frequency interpolation scheme (Stolt mapping).

The applicability of the techniques above span from coarse resolution data, on to fine resolution NB data and finally on to fine resolution UWB data.

Frequency domain algorithms assume a linear track, known deviations are then compensated locally (motion compensation, e.g. to a scene or a swath centre, see [3]). The validity however deteriorates as deviations intensify (especially for UWB systems), possibly defocusing the final image.

[1] Note that a (azimuth) Fourier transform performs azimuth compression in the DBS case, the rectangular algorithm in turn applies 1-dimensional matched filters in range and azimuth, increasing the accuracy.

[2] For squinted geometries and/or wide integration angles, defocusing range-azimuth phase effects appear, encouraging a compensation labeled as a Secondary Range Compression (SRC).

[3] As opposed to the Rectangular Format Algorithm (RFA) [3,21,32], a performance restricted PFA approximation.

[4] In the RD domain; targets at the same range of closest approach share a single trajectory, facilitating RCMC.

As mentioned before, the run time has been the main motivation for frequency domain SAR processing. Recent studies [19,23,31,35,36,43] have however proposed strategies to speed up the time domain approach. Adding the ability to deal with data acquired along a nonlinear track, by an arbitrary system, accurately (presuming that deviations are known), makes (certain) time domain algorithms a feasible, or for some scenarios even a superior substitute.

Two time domain techniques will now be resumed, to lay a foundation for the third chapter, or more specifically for the new autofocus approach.

Note that the algorithms are described in discrete terms, as opposed to the matched filter formulation in chapter 1. It is presumed that samples (in fast- and slow-time) are taken frequently enough to satisfy the Nyquist theorem, the criteria (for complex sampling) are: $1/\Delta\tau > B$ and $1/\Delta\eta > B_d$. The Pulse Repetition Frequency (PRF) sets the slow-time interval ($\Delta\eta$). If the PRF violates Nyquist, azimuth ambiguities occur, if the PRF is too high ($1/\Delta\eta > c/2R_{max}$), range ambiguities arise. This complicates the data collection.

2.2 Global Back-Projection

Global Back-Projection (GBP)[5] [1,8,12,27,32,36] is a mathematically equivalent solution to the matching strategy in the previous chapter, reducing the computational effort (but not sufficiently).

GBP basically projects range compressed radar echoes to a generally defined Image Display Plane (IDP). Each slow-time position along a track contributes with a data value to each and every pixel. Complex values are added coherently, causing interference, resolving reflective structures.

Equation (2.1) gives a BP expression, while (2.2) represents slant range:

$$I(x,y) = \sum_{n=1}^{N} f(n, R(n)) \cdot R(n) \cdot e^{j4\pi R(n)/\lambda_c} \tag{2.1}$$

$$R(n) = \sqrt{(x_n - x)^2 + (y_n - y)^2 + (z_n - z)^2} \tag{2.2}$$

In (2.1); I is an image, formed from data acquired along an arbitrary track (extending across N sample positions). The slant range ($R(n)$) between the platform position (x_n, y_n, z_n) and the pixel (x, y, z)[6] in question, determines which data value ($f(n, R(n))$) to accumulate; range interpolation retrieves the proper value from available samples. For demodulated data, each value must also be multiplied by a phase factor (the exponential). The range multiplication is in turn included to establish a $1/R$ dependence[7].

To summarize; GBP is a versatile algorithm (dealing with nonlinear tracks, topography etc.), however, the number of operations (proportional to N^3 for N sample positions and an $N \times N$ image) normally restricts its use to moderately sized images.

It should also be stressed, that in appended papers the BP principle is employed to process partial tracks, i.e. to form sub-images.

2.3 Fast Factorized Back-Projection

Fast Factorized Back-Projection (FFBP) is a time efficient alternative to GBP, utilizing a coherent combination scheme to merge range compressed radar echoes stage by stage. In principle, the track is partitioned into sub-apertures, increasing in length (finer angular resolution) and decreasing in number for each factorization step [36]. Every sub-aperture comes with a corresponding sub-image.

The factorization can be realized in various ways[8]. Polar FFBP divides the antenna beam into sub-lobes, forming images with pixels in range and sub-lobe angle. (this indicates that the scheme involves interpolation in both range and angle [15,36]) Ideally[9], the final factorization step yields the aperture image.

[5] Referred to as convolution, filtered and tomographic Back-Projection (BP) (or just BP) in [1,8,12,27,32,36].
[6] z is either a DEM coordinate or a constant.
[7] Note that this formulation omits a ramp filter, applied to even out the spectrum, for further details see [36].
[8] For example: Polar FFBP and Block FFBP [36].
[9] Presuming that the number of (slow-time) positions is expressible as a factorization of integers.

Equation (2.3) gives a base two FFBP expression:

$$G(r,\theta) = G_1(r_1,\theta_1)\cdot e^{j4\pi(r-r_1)/\lambda_c} + G_2(r_2,\theta_2)\cdot e^{j4\pi(r-r_2)/\lambda_c} \tag{2.3}$$

In (2.3); G is a sub-image or an aperture image, formed by adding contributions (G_1 and G_2) from the prior factorization step. The pixel (r,θ) with origin at the centre of the sub-aperture has a corresponding FTP point on the ground (assumed horizontal again). (r_1,θ_1) and (r_2,θ_2) are polar coordinates of vectors, extending from preceding centres to the ground point, angles are defined with respect to sub-aperture vectors. Data values are determined by the coordinates and retrieved from available samples through interpolation. As in (2.1), exponentials account for demodulation.

For a base two implementation, the number of operations is proportional to $N^2\log_2 N$ [36] (for N sample positions and an $N\times N$ image), i.e. under the premise that N equals a power of two. However, image quality requirements may demand a less effective algorithm execution (e.g. by reducing the number of FFBP steps and/or using a more exact interpolator), to make up for the fact that interpolation (phase) errors are accumulated for each factorization step (for further details see [15, 36]).

Chapter 3

Autofocus

3.1 Stand-Alone Autofocus - An Overview

Since the early 70's, numerous parametric and non-parametric autofocus techniques have been developed. Most of these are as mentioned 1-dimensional, addressing phase errors in azimuth by applying a correction factor in the RD domain. An overview of the work done in the field follows.

MapDrift Algorithms

MapDrift (MD) [3, 21] is a widely used parametric autofocus technique, with the ability to correct quadratic phase errors. The algorithm first divides an aperture into two sub-apertures, intensity sub-images are formed and range bins with strong targets (in both sub-images, i.e. range bin pairs) are cross-correlated. For any bin pair, the correlation lag giving a similarity peak indicates a sub-image off-set. By averaging all lags (giving similarity peaks) the relative shift is found. This shift is proportional to the (presumed) error coefficient. Range bins (in the RD domain) are multiplied by the complex conjugate of the estimated component, an inverse (azimuth) Fourier transform then finally yields the image (ideally focused). Iterating the MD procedure may refine the result.

If the aperture is divided into more than two sub-apertures, i.e. Multiple Aperture MD (MAMD) [3, 21], phase errors of higher order may be modeled as well (three sub-apertures can for example also model a cubic component). The order is however limited in practice (approximately to the fifth order), as shorter sub-apertures imply a degradation of resolution and SNR. A less recognized MD related routine is the Phase Difference Algorithm (PDA) [3], cross-correlating complex image bins (in the RD domain) instead[1]. Lately a coherent MD approach has also appeared in the literature [30].

Phase Gradient Algorithms

The Phase Gradient Algorithm (PGA) [3, 10, 11, 20, 21, 40] is a notable non-parametric autofocus technique, with the ability to correct high order phase errors. The algorithm involves a number of sequential steps, typically iterated to attain convergence. First strong targets (in individual range bins) are identified in a defocused image. These are aligned through a circular shift and windowed to discard extraneous data. Next an expression for the phase error derivative (averaged over the bins) is found in the RD domain. Integrating this expression gives an estimate of the error. Range bins are multiplied by the complex conjugate of the estimate; ideally, this eliminates the phase errors. Finally bins are transformed back to the time domain. The PGA principle has been proven to be robust for a diversity of different scenes and though many alternative schemes have been suggested (a routine increasing the rate of convergence is for example described in [4]), the conventional PGA formulation is still the standard; its vast use within the SAR community has even made it a norm for emerging autofocus strategies. Defocused and PGA processed images are shown in figure 3.1, the examples support the coming section.

[1] All bins used to reach a good result on the first try.

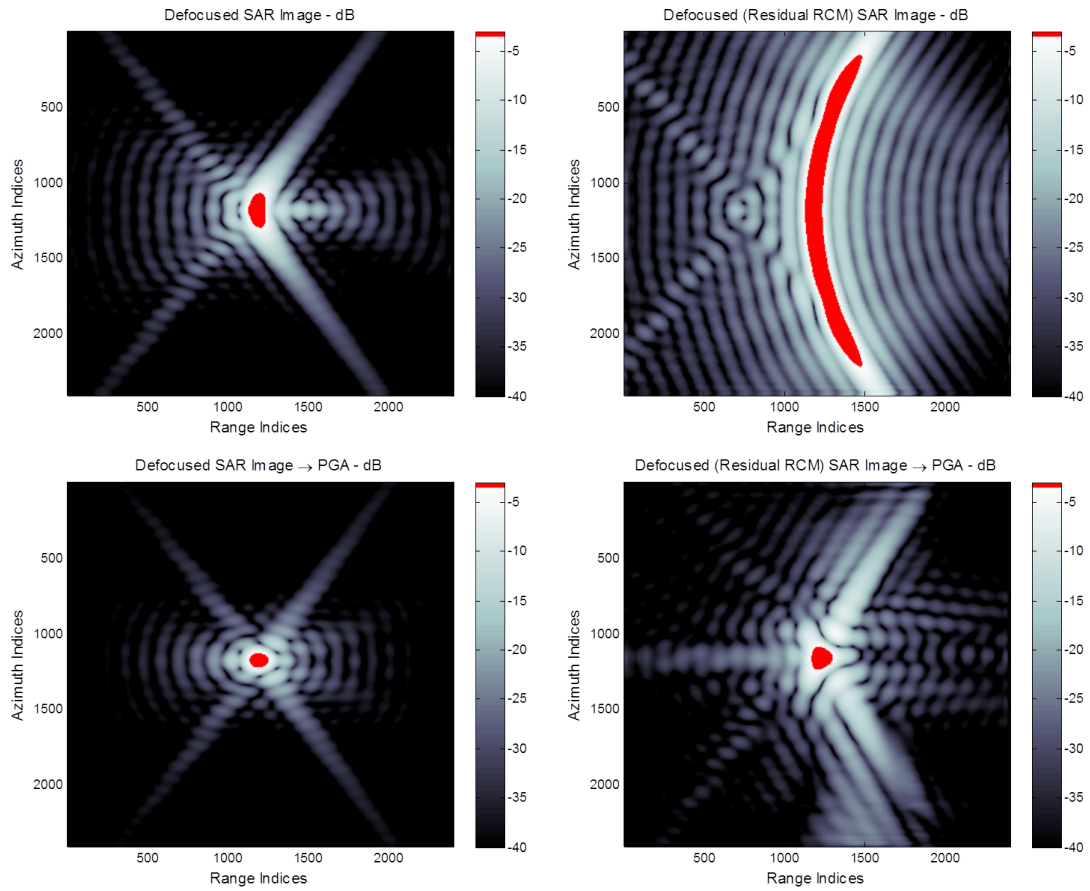

Figure 3.1: shows a defocused image (top left) of a target (compare to figure 1.4 (left)), a linear track in the horizontal plane is read, however, the track is really curved quadratically (in the plane). Essentially, motion measurement errors generate false phase components (approximately quadratic and 1-dimensional), blurring the mainlobe (primarily) in azimuth. If the curvature is increased phase errors become 2-dimensional. The top right image illustrates a target suffering the consequences of residual RCM, a challenging SAR issue. The PGA almost corrects the left image (measurements reveal a minor mainlobe broadening and a PSLR degradation), the right image is not easily compensated; the result is not acceptable.

Metric-Based Algorithms

Apart from MD and PGA techniques, metric-based algorithms [13, 14, 22, 44] (spanning the space of both parametric and non-parametric techniques) are gaining more and more attention. The idea is to try out different (phase) correction factors (on range bins in the RD domain). An object function provides a focus measure for each trial. If a measure is deficient, the factor is altered and applied again. This procedure is repeated until a focused image is obtained. Though the strategy potentially can produce better results than MD and PGA techniques (at a reasonable run time), numerous questions normally arise, for example regarding the choice of object function (e.g. contrast [22], entropy [44], squared intensity [13, 14], etc.) and optimization routine (to find a good fit (factor) as fast as possible).

3.2 Limiting Premises & Present Solutions

Standard autofocus techniques are as stressed 1-dimensional, presuming that phase errors reside in individual range bins [3, 18]. Essentially this implies, that after SAR processing, there can be no residual RCM (see figure 3.1 (right)). In addition, phase errors are usually assumed invariant in space [3,18]. These restrictions are not by necessity well-founded[2], especially not if motion measurement errors are allowed to escalate (relaxed requirements on the GPS/INS/IMU.). However, still, at this point in time; limiting premises laid down by 1-dimensional autofocus techniques have only been partially dropped [18].

The 2-dimensional PGA [16, 42] can mitigate residual space invariant RCM. An alternative approach is to first apply a 1-dimensional PGA realization on a coarse range resolution image, essentially estimating and removing RCM prior to fine range compression. The algorithm is then applied again to correct remaining (1-dimensional) phase errors. This strategy (and a similar semi-integrated PGA strategy) is described in [9].

Space variant effects may be eased by breaking up a defocused image into space invariant areas [3]. These are then processed separately and patched to form a focused image. Naturally though, estimation accuracy deteriorates as the areas decrease in size. Additionally, border defects may arise (i.e. a penalty for patching).

Residual space variant RCM is a demanding autofocus problem, the schemes above can be combined in an attempt to solve it. Disadvantages lifted in the previous paragraph are however inherited. Prominent Point Processing (PPP) [3] also has the potential to relieve the issue. (i.e. by tracking several targets in a defocused image and using deduced information to model the phase errors). Though the routine is hard to automatize and it relies on strong point-like targets (ideally, scattered and isolated).

This thesis however, presents a possible solution to the problem; an autofocus algorithm, regulating track parameters in the time domain. The proposed strategy omits reported restrictions, implying a capacity to correct an arbitrary inaccurate geometry (from a focusing perspective) and in consequence residual space variant RCM.

3.3 Geometrical Autofocus - Summary of Appended Papers

The novel strategy, refered to as the Factorized Geometrical Autofocus (FGA) algorithm in paper B, is integrated in a base two FFBP chain, processing data in a horizontal plane. The FGA approach fundamentally relies on varying geometry parameters stage by stage to obtain a sharp image. Focus measures are provided by an object function (intensity correlation), correlating sub-image contributions (see G_1 and G_2 in (2.3)). For a general autofocus problem six independent track parameters are required. However, in the appended papers, constrained problems involving one parameter are devised, merely to demonstrate the capacity of the algorithm in a clear manner.

In paper A the FGA algorithm is applied on a simulated (point targets without noise) UWB data set. Basically the geometry is modified prior to processing to imitate motion measurement errors. In this case, data is generated along a curved track. The cross-track acceleration is however ignored (a linear track is assumed), inducing 1-dimensional (azimuth) defocusing effects.

In paper B the FGA algorithm is applied on two simulated (point targets with and without noise) and two real (CARABAS II) UWB data sets. For simulated data the track length (linear tracks) is altered. The track scale (nonlinear tracks) is in turn adjusted for real data. In this paper, erroneous geometries induce critical defocusing effects (compared to the effects in paper A), i.e. residual space variant RCM.

FGA images are compared to reference images and to defocused images. In paper B, PGA processed images are also included in the evaluation, to be able to benchmark the geometrical approach against a standard algorithm. Apart from a visual analysis, resolution and PSLR are also assessed. FGA images resemble corresponding reference images, verified further by the fact that resolution (3-dB in azimuth and range) and PSLR disparities are limited to a few percents and tenths of a dB (for point targets and point-like targets (real images)). PGA images (paper B) are on the contrary not acceptable, as defocusing effects still are observed.

[2] In particular not for airborne UWB SAR systems.

Chapter 4

Conclusions & Future Work

4.1 Conclusions

This thesis describes the principle of SAR and the fundamental image formation approach, resolving the scene reflectivity from raw data. After a brief review of basic concepts, different processing techniques and (standard) autofocus strategies are summarized. The primary topic is then introduced, i.e. autofocus in the time domain.

Standard autofocus strategies can only correct space invariant phase errors in one dimension. The call for fine resolution imagery and relaxed requirements on measurement accuracy (GPS/INS/IMU) may on the contrary introduce space variant phase errors in two dimensions (residual space variant RCM). Thus, there is a need for a new autofocus approach, with the ability to correct arbitrary (geometrical) phase errors.

A capable algorithm can be realized by integrating a geometrical alteration procedure in a conventional FFBP chain, i.e. in the time domain. By adjusting six independent (geometry) parameters stage by stage, motion measurement errors may be compensated completely, giving a focused image.

The novel strategy is labeled (paper B) as the Factorized Geometrical Autofocus (FGA) algorithm. In appended papers, the FGA algorithm is resumed (paper A and B) and derived in detail (paper B). The potential of the algorithm is also proven (for constrained problems), by relieving residual space variant RCM for simulated and real (CARABAS II) data sets (paper B)[1].

To sum up; results presented in the papers are satisfying. Thus it is concluded that the FGA algorithm can correct an inaccurate geometry and consequential phase errors. The run time must be reduced though, before devising a more realistic autofocus problem.

4.2 Future Work

The run time is recognized as the main obstacle in the appended papers. A sensitivity characterization in relation to independent parameters should be able to reveal, if all the quantities really are required to retain focus at the FFBP step in question. The exhaustive search routine (utilized in paper A and B to find the best geometry fit) must in turn be replaced by a faster alternative. Gradient descent based schemes should be surveyed.

The focus measure[2] (the object function) is also an interesting subject. Though intensity correlation has performed well thus far, there are numerous other object functions to consider, e.g. contrast, squared intensity, entropy, etc.

How to select a suitable image area (or more likely, image areas) for focus measurements is a related matter. From a run time perspective, it is not feasible to apply the object function on full images. In practice areas should be minimized without risking the reliability of the search. If areas suggest different geometries,

[1] In paper A, space invariant phase errors residing in separate range bins are compensated (simulated data).

[2] A measure deciding if the image is focused by the current geometry hypothesis

the hypotheses must be merged to a single geometry solution in some way (averaging is a possibility), basically to avoid a purely local compensation.

Apart from FGA specific issues above, interpolation tactics and the incorporation of a DEM (both in context of the FGA algorithm and conventional (polar) FFBP processing) are also future research themes.

References

[1] L-E. Andersson. On the determination of a function from spherical averages. *Siam J. Math. Anal.*, 19(1):214–232, 1988.

[2] C. Cafforio, C. Prati, and F. Rocca. SAR data focusing using seismic migration techniques. *IEEE Transactions on Aerospace and Electronic Systems*, 27(2):194–207, 1991.

[3] W. G. Carrara, R. S. Goodman, and R. M. Majewski. *Spotlight Synthetic Aperture Radar: Signal Processing Algorithms*. Artech House Inc, Norwood, Ma, 1995.

[4] H. L. Chan and T. S. Yeo. Noniterative quality phase gradient autofocus (QPGA) algorithm for spotlight SAR imagery. *IEEE Transactions on Geoscience and Remote Sensing*, 36(5):1531–1539, 1998.

[5] I. G. Cumming and F. H. Wong. *Digital Processing of Synthetic Aperture Radar Data: Algorithms and Implementation*. Artech House Inc, Norwood, Ma, 2005.

[6] I. G. Cumming, F. H. Wong, and R. K. Raney. A SAR processing algorithm with no interpolation. In *Proceedings of International Geoscience and Remote Sensing Symposium, IGARSS'92*, pages 376–379, Clear Lake, TX, 1992.

[7] G. W. Davidson, I. G. Cumming, and M. R. Ito. A chirp scaling approach for processing squint mode SAR data. *IEEE Transactions on Aerospace and Electronic Systems*, 32(1):121–133, 1996.

[8] M. D. Desai and K. W. Jenkins. Convolution backprojection image reconstruction for spotlight mode synthetic aperture radar. *IEEE Transactions on Image Processing*, 1(4):505–517, 1992.

[9] A. W. Doerry. Autofocus correction of SAR images exhibiting excessive residual migration. In *Proceedings of SPIE Radar Sensor Technology IX*, pages 34–45, 2005.

[10] P. H. Eichel, D. C. Ghiglia, and C. V. Jakowatz. Speckle processing method for synthetic-aperture-radar phase correction. *Optics Letters*, 14(20):1–3, 1989.

[11] P. H. Eichel and C. V. Jakowatz. Phase-gradient algorithm as an optimal estimator of the phase derivative. *Optics Letters*, 14(20):1101–1103, 1989.

[12] J. A. Fawcett. Inversion of N-dimensional spherical averages. *Siam J. Math. Anal.*, 45(2):336–341, 1985.

[13] J. R. Fienup. Synthetic-aperture radar autofocus by maximizing sharpness. *Optics Letters*, 25(4):221–223, 2000.

[14] J. R. Fienup and J. J. Miller. Aberration correction by maximizing generalized sharpness metrics. *J. Opt. Soc.*, 20(4):609–620, 2003.

[15] P-O. Frölind and L. M. H. Ulander. Evaluation of angular interpolation kernels in fast back-projection SAR processing. In *Proceedings of IEE Radar, Sonar and Navigation*, volume 153, pages 243–249, 2006.

[16] D. C. Ghiglia and G. A. Mastin. Two-dimensional phase correction of synthetic-aperture-radar imagery. *Optics Letters*, 14(20):1104–1106, 1989.

[17] H. Hellsten and L-E. Andersson. An inverse method for processing synthetic aperture radar data. *Inverse Problems*, 3:111–124, 1987.

[18] H. Hellsten, P. Dammert, and A. Åhlander. Autofocus in fast factorized back-projection for processing of SAR images when geometry parameters are unknown. In *Proceedings of IEEE Radar Conference*, pages 603–608, Washington, DC, 2010.

[19] H. Hellsten, L. M. H. Ulander, A. Gustavsson, and B. Larsson. Development of VHF CARABAS II SAR. In *Proceedings of SPIE Radar Sensor Technology*, pages 48–60, Orlando, FL, 1996.

[20] C. V. Jakowatz and D. E. Wahl. Eigenvector method for maximum-likelihood estimation of phase errors in synthetic-aperture-radar imagery. *Optics Letters*, 10(22):2539–2546, 1993.

[21] C. V. Jakowatz, D. E. Wahl, P. H. Eichel, D. C. Ghiglia, and P. A. Thompson. *Spotlight-Mode Synthetic Aperture Radar: A Signal Processing Approach*. Springer Science Inc, New York, NY, 1996.

[22] J. Kolman. PACE: an autofocus algorithm for SAR. In *Proceedings of IEEE International Radar Conference*, pages 310–314, 2005.

[23] J. McCorkle and M. Rofheart. An order $N^2 \log(N)$ backprojector algorithm for focusing wide-angle wide-bandwidth arbitrary-motion synthetic aperture radar. In *Proceedings of SPIE AeroSense Conference*, pages 25–36, Orlando, FL, 1996.

[24] A. Moreira and Y. Huang. Airborne SAR processing of highly squinted data using a chirp scaling approach with integrated motion compensation. *IEEE Transactions on Geoscience and Remote Sensing*, 32(5):1029–1040, 1994.

[25] A. Moreira, J. Mittermayer, and R. Scheiber. Extended chirp scaling algorithm for air- and spaceborne SAR data processing in stripmap and scanSAR imaging modes. *IEEE Transactions on Geoscience and Remote Sensing*, 34(5):1123–1136, 1996.

[26] R. K. Raney, H. Runge, R. Bamler, I. G. Cumming, and F. H. Wong. Precision SAR processing using chirp scaling. *IEEE Transactions on Geoscience and Remote Sensing*, 32(4):786–799, 1994.

[27] M. A. Richards, J. A. Scheer, and W. A. Holm. *Principles of Modern Radar: Basic Principles*. SciTech Publishing Inc, Raleigh, NC, 2010.

[28] F. Rocca, C. Cafforio, and C. Prati. Synthetic aperture radar: a new application for wave equation techniques. *Geophysical Prospecting*, 37:809–830, 1989.

[29] H. Runge and R. Bamler. A novel high precision SAR focusing algorithm based on chirp scaling. In *Proceedings of International Geoscience and Remote Sensing Symposium, IGARSS'92*, pages 372–375, Clear Lake, TX, 1992.

[30] P. Samczynski and K. S. Kulpa. Coherent mapdrift technique. *IEEE Transactions on Geoscience and Remote Sensing*, 48(3):1505–1517, 2010.

[31] O. Seger, M. Herberthson, and H. Hellsten. Real-time SAR processing of low frequency ultra wide band radar data. In *Proceedings of EUSAR*, pages 489–492, Friedrichshafen, Germany, 1998.

[32] M. Soumekh. *Synthetic Aperture Radar Signal Processing with MATLAB Algorithms*. John Wiley & Sons Inc, New York, NY., 1999.

[33] R. J. Sullivan. *Radar Foundations for Imaging and Advanced Concepts*. SciTech Publishing Inc, Raleigh, NC, 2004.

[34] L. M. H. Ulander and H. Hellsten. A new formula for SAR spatial resolution. *International Journal of Electronics and Communications*, 50(2):117–121, 1996.

[35] L. M. H. Ulander, H. Hellsten, and G. Stenström. Synthetic-aperture radar processing using fast factorized backprojection. In *Proceedings of EUSAR*, pages 753–756, Munich, Germany, 2000.

[36] L. M. H. Ulander, H. Hellsten, and G. Stenström. Synthetic-aperture radar processing using fast factorized back-projection. *IEEE Transactions on Aerospace and Electronic Systems*, 39(3):760–776, 2003.

[37] V. T. Vu, T. K. Sjögren, and M. I. Pettersson. Ultrawideband chirp scaling algorithm. *IEEE Geoscience and Remote Sensing Letters*, 7(2):281–285, 2010.

[38] V. T. Vu, T. K. Sjögren, and M. I. Pettersson. On synthetic aperture radar azimuth and range resolution equations. *IEEE Transactions on Aerospace and Electronic Systems*, 48(2):1764–1769, 2012.

[39] V. T. Vu, T. K. Sjögren, M. I. Pettersson, and H. Hellsten. An impulse response function for evaluation of ultrawideband SAR imaging. *IEEE Transactions on Signal Processing*, 58(7):3927–3932, 2010.

[40] D. E. Wahl, Eichel, P. H., D. C. Ghiglia, and C. V. Jakowatz. Phase gradient autofocus-a robust tool for high resolution SAR phase correction. *IEEE Transactions on Aerospace and Electronic Systems*, 30(3):827–834, 1994.

[41] J. L. Walker. Range-Doppler imaging of rotating objects. *IEEE Transactions on Aerospace and Electronic Systems*, AES-16(1):23–52, 1980.

[42] D. W. Warner, D. C. Ghiglia, A. FitzGerrell, and J. Beaver. Two-dimensional phase gradient autofocus. In *Proceedings of SPIE Image Reconstruction from Incomplete Data*, pages 162–173, 2000.

[43] A. F. Yegulalp. Fast backprojection algorithm for synthetic aperture radar. In *Proceedings of IEEE Radar Conference*, Waltham, MA, 1999.

[44] A. F. Yegulalp. Minimum entropy SAR autofocus. In *ASAP '99 Workshop*, 1999.